

INDIRECT TISSUE SCAFFOLD FABRICATION VIA FUSED DEPOSITION MODELING AND BIOMIMETIC MINERALIZATION

Jesse Bernardo¹, Satyavrata Samavedi², Christopher B. Williams^{1,3*}, Abby R. Whittington^{2,4}

¹ Department of Mechanical Engineering, ² Department of Chemical Engineering, ³ Department of Engineering Education, ⁴ Department of Materials Science and Engineering
Virginia Polytechnic Institute and State University

REVIEWED, August 17 2011

ABSTRACT

To alleviate material limitations of the additive manufacture of tissue scaffolds, researchers have looked to indirect fabrication approaches. The feature resolution of these processes is limited however, due to the viscous ceramic slurries that are typically employed. To alleviate these limitations, the authors look to an indirect fabrication process wherein a pattern, created using Fused Deposition Modeling, is biomimetically mineralized with an aqueous simulated body fluid, which forms a bonelike hydroxyapatite throughout the scaffold pattern. Mineralized patterns are then heat treated to pyrolyze the pattern and sinter the minerals. With this process, scaffolds were created with wall thicknesses as small as 150 μm and internal channel diameters of 280-340 μm , an appropriate range for bone tissue engineering.

Keywords: Fused Deposition Modeling, Biomimetic Mineralization, Tissue Scaffold, Additive Manufacturing

1. TISSUE SCAFFOLDS WITH DESIGNED MESOSTRUCTURE

A tissue scaffold is an artificial cellular structure composed of a biocompatible material that mimics a body's extra-cellular matrix (ECM) and supports three-dimensional tissue formation in order to begin healing an injury [1-3]. The scaffold's internal structure (featuring interconnected pores and channels) provides surface area for cell attachment and pathways for cell movement [4, 5], surface area for cell attachment, diffusion of nutrients, and removal of cell wastes within the scaffold. In addition, it provides mechanical and chemical cues that affect the cellular ingrowth, differentiation, and vascularization [6-8].

The mesostructure of the scaffold (i.e., the size, orientation and geometry of the scaffold pores) can affect its ability to mimic the ECM and thus affects how well cells proliferate throughout the structure [9-11]. Several researchers have found that different cell types prefer different scaffold structures, with porosity and pore size being the most commonly benchmarked properties. Scaffolds with a high porosity offer more "living space" for cells to move into and start to grow. Scaffold porosity should be greater than 75% to ensure cell proliferation [9]; however, the maximum porosity is limited by the required mechanical strength of the scaffold – a key tradeoff in the design and fabrication of tissue scaffolds. Furthermore, pores that are too small will become clogged and cause a decrease in nutrient diffusion, cellular penetration, ECM production, neovascularization [4] and possibly cell death; pores that are too large form gaps that the cells cannot cross. Pore sizes on the range of 200-400 micrometers are accepted for bone cell proliferation [1, 12, 13].

Although porosity and pore size provide the living space and pathways for cell movement, the scaffold's permeability affects how nutrients are delivered to, and wastes are removed from, the cells. Ku et al. suggest that permeability is a combination of several scaffold factors including: porosity, pore size, distribution and orientation, and interconnectivity [14]. The tissue scaffolds' permeability should provide nutrients until a vascular system is in place [11]. Once a vascular system exists throughout the scaffold, cell nutrient and waste removal is carried through the blood vessels.

Microscale topology can also affect cell behavior within the scaffold. Specifically, surface topography will influence cellular attachment, movement and cellular signaling [15]. The scaffold's bulk crystallinity [16], surface roughness [4] and microporosity [10] are known to affect cellular attachment, proliferation and migration and neovascularization.

* Corresponding Author: 114F Randolph Hall, Blacksburg, VA, 24061; cbwilliams@vt.edu; (540) 231-3422

Finally, the mechanical properties of the scaffold should match those of the tissue it is replacing; this will protect the cells from mechanical loads, contractile forces from tissue formation [17], and any in vivo/vitro stresses [15, 18].

Thus, scaffold structure should be designed to support specific cell types in order to maximize the growth potential of the desired tissue [8, 15]. However, existing scaffold fabrication techniques do not permit this level of design freedom. While stochastic fabrication techniques (e.g. solvent casting and particle leaching [19], gas foaming [20, 21], and emulsification, freeze-drying and thermally induced phase separation [22-24]) processes result in highly porous scaffolds, the size, shape, location and orientation of the porosity is stochastic, and thus is unable to provide repeatable results. Furthermore, these methods are process dependent and do not allow for the strategic placement of material, and therefore do not allow for control over pore placement and internal architecture.

Additive Manufacturing (AM) technologies' precise control of pore size, geometry, interconnectivity and distribution throughout the scaffold affords the creation of scaffold mesostructures that are designed for specific tissues [25]. Many different AM methods have been used to create biocompatible scaffolds (as reviewed in the authors' prior work [26]). 3D Printing has been used to create PLGA scaffolds [27, 28]. Scaffolds made of ceramics (e.g., hydroxyapatite [29] and calcium phosphate [30]), biodegradable polymers [31], and hydrogels [32] have been created by stereolithography (SL) techniques. Laser sintering (LS), which uses a laser to selectively fuse together powder particles in a powder bed, has been used to create scaffolds made of ceramic/polymer blends such as polymer-coated calcium phosphate [33, 34] and hydroxyapatite [35].

While each of these AM technologies is capable of producing scaffolds with controlled geometry and porosity with repeatable results, they do suffer from some processing limitations. The primary limitation is the relatively few biocompatible materials that are compatible with each system – materials available to AM techniques are mostly constrained to polymers that are specialized for each process. For example, SL scaffold fabrication is limited to materials that can be cured by UV irradiation, thus limiting its ability to directly fabricate scaffolds for hard tissue [36]. Extrusion processes are limited to materials that can be melted into a semi-liquid phase before extrusion [37]. Many researchers have tried to extend the processes' working materials by integrating bio-compatible ceramic particles into polymer systems as in LS [38, 39], SL [40-42], and Robocasting [43, 44]. However, the resultant parts suffer from a reduced resolution and pore size [41, 45], and delamination, cracking and warping as the large concentrations of polymeric binder are pyrolyzed [40, 46, 47].

To bypass these material limitations, indirect fabrication techniques (i.e., investment casting approaches) have been proposed; however, their reliance on viscous ceramic slurries prevents the realization of scaffold geometries with fine features (Section 2). In this paper the authors detail their exploration of an indirect scaffold fabrication process wherein biomimetic ceramic mineralization is used to coat scaffold patterns that are fabricated by additive manufacturing. The process alleviates both the material and geometric limitations imposed by existing scaffold fabrication techniques. An overview of the indirect fabrication process is provided in Section 3. Experimental methods are described in Section 4. In Section 5, the results of process experimentation are provided. Finally, closure and opportunities for future work are described in Section 6.

2. INDIRECT FABRICATION OF SCAFFOLDS

Indirect scaffold fabrication techniques have been explored as a means of circumventing the inherent material processing limitations of existing AM techniques. Existing indirect scaffold fabrication techniques typically follow a strategy similar to investment casting. First, a negative mold of the desired scaffold is fabricated, into which a biocompatible slurry is cast. The slurry contains the scaffold material (e.g., HA, PLGA, collagen), solvents (e.g., chloroform and methanol), and porogens [48-50]. The slurry is then solidified via a curing process. After the slurry has set, the mold is removed – leaving behind a biocompatible scaffold with internal channels.

Hydroxyapatite (HA) macro-porous scaffolds have been created by using SLA [49] and 3DP [51] to create negative molds. After mold fabrication, a HA slurry is cast and dried in the mold. The cast is heated to remove mold material and then sintered (around 1300 °C) to increase the density of the HA. The wall thicknesses created from the mold process were not smaller than other AM techniques: SLA molds were 800 – 1200 μm; 3DP molds were 500 μm. In addition, these HA scaffolds did not contain a “local” pore distribution.

Sachlos et al. fabricated porous biocompatible collagen scaffolds with channels by casting a collagen/water solution into a mold printed by a Model Maker II (Figure 1) [52]. No new material formulation for printing the mold was necessary; the machine manufacturer's printing mediums (ProtoBuild™ and ProtoSupport™) were used. After fabricating the mold, the ProtoSupport™ material is removed by submerging the mold in a solvent (BioAct™) to create a negative mold. The collagen suspension was cast into the mold and frozen (–20 °C) to form a tissue

scaffold. The mold and scaffold were then immersed in ethanol, which dissolved the mold material and ice crystals. Critical point drying was used to remove any remaining solvents and ice crystals. Shrinkage during critical point drying reduced the accuracy of the printed channels. An increase in collagen dispersion in the cast suspension decreases shrinkage [52] but is limited because an increase in viscosity can prevent the collagen suspension from penetrating small channels. Although some scaffolds were designed to have a channel width of 150 μm , the smallest channel widths reported for this processes were $181 \pm 8 \mu\text{m}$.

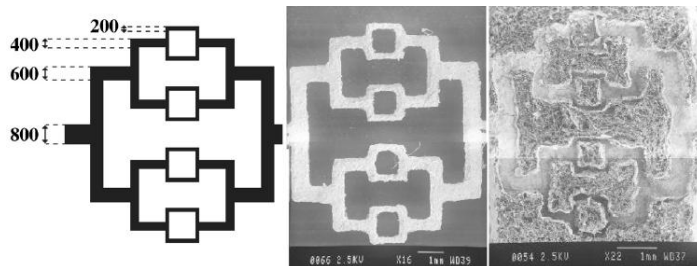


Figure 1. A) Designed channel width. B) Printed mold with varying channel widths. C) Porous collagen mold with designed channel widths. [52].

In a similar manner, Yeong et al. fabricated biocompatible collagen scaffolds by casting a collagen/water solution into a mold printed by an inkjet printer (Solidscap’s T612 Benchtop) [50]. No new formulation of mold material was needed and the machine’s original printing mediums (InduraCast and Indurafill) were used to print the mold. The collagen suspension was frozen in the mold ($-20 \text{ }^\circ\text{C}$) and then immersed in ethanol to dissolve the mold [53]. The scaffold was then freeze-dried to remove water crystals from the collagen suspension leaving behind randomly oriented pores ($191 \pm 50 \mu\text{m}$) [53]. A branched channel design with channel widths of 200 and 300 μm was achieved.

Lee et al. fabricated collagen scaffolds with “villa” like features [54] using 3DP to create a plaster mold. The plaster mold was infiltrated with PEG to increase its strength before the mixture of PLGA, chloroform, methanol and sucrose was cast. The PLGA cast was dried in a fume hood before being immersed in deionized water. Water dissolved the mold and sucrose (which acted as a porogen) to leave behind porous “villa” like features that tapered from $\sim 700 - 500 \mu\text{m}$ in diameter and 1 mm high. The pores that formed from leaching sucrose ($\sim 100 - 150 \mu\text{m}$) were uniformly distributed and well connected [54].

Taboas et al. [55] fabricated “multi-pore-architecture” poly(L)lactide (PLA) scaffolds that contained controlled macro-pores (interconnected macro-pores 600 μm in diameter) with local porosity (50 – 100 μm) created by particle leaching (Figure 2). Macro-pores may increase diffusion of nutrients to cells deep in the scaffold while local pores provide living space for the cells [55].

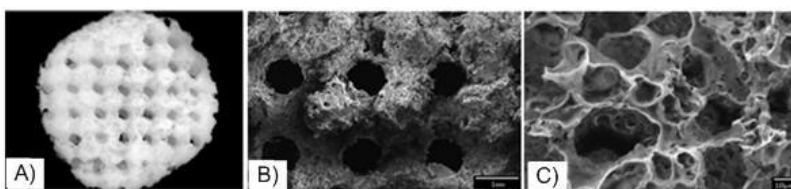


Figure 2. A) PLA scaffold with designed macro-pores and local pores. B) Designed macro-pores are interconnected (in a three-dimensional structure) cylindrical channels. C) SEM of local porosity created by salt leaching [55].

The use of AM to manufacture molds presents three important contributions to the design of tissue scaffolds:

- *Using molds relaxes the material limitations associated with AM.* The mold material does not have to be biocompatible, thus scaffolds can be fabricated “from the largest pool of materials available [55].” Also, materials that are already compatible for the AM machine can be used instead of developing new materials [51].
- *Allows for the simultaneous creation of macro-pores (channels) and local pores (porogen)* [55]. AM molds can produce scaffolds with designed internal channels and may increase cell viability in solvent-cast/porogen-leach scaffolds [52] by increasing the nutrient flow to cells in the scaffold.
- *Toxic/residual materials can be removed more easily from the scaffold.* Whereas “solvent casting and particle leaching” methods were limited by thickness, indirect methods contain macro-pores which enhance the removal

of mold material. Macro-pores allow the removal of toxic solvents, and porogens from the scaffold allowing scaffolds to be fabricated with thicker cross sections [55].

Typical restrictions of traditional casting processes, imposed by an inability to fabricate molds that would result in complex geometry and internal architecture, are alleviated by fabricating molds via AM [56]. However, existing indirect fabrication approaches do limit the features that are able to be produced. In general, the processes are limited by:

- *Non-cell friendly separation of mold from the cast.* The mold materials must be completely removed from the cast material without compromising the scaffold architecture. Harsh chemicals and extreme temperatures can remove the mold while leaving the cast intact but prohibit the incorporation of living cells or growth hormones.
- *Weak mechanical properties* due to the creation of local pores within the scaffold architecture.
- *Mold imperfections are transferred to the cast* [55].
- *Increased fabrication time.* Scaffolds take longer to make than direct-fabrication AM because a mold must be fabricated, cast, and dissolved.
- *Feature resolution is limited by the viscosity of the cast material.* Viscous materials, such as high loaded ceramic suspensions, may trap air bubbles within the mold and cause defects in the scaffold architecture [53]. As a result of the viscosity limitations the internal channels and scaffold walls (366 and 800 μm [2]) are larger than other AM produced scaffolds.

Alleviating the existing limitations of indirect scaffold fabrication approaches is of merit, as doing so will allow the realization of designed scaffold structures that are not constrained to specific geometries or materials.

3. INDIRECT FABRICATION OF SCAFFOLDS VIA ADDITIVE MANUFACTURING AND BIOMIMETIC MINERALIZATION

While indirect AM approaches to scaffold fabrication alleviate limitations imposed by traditional stochastic fabrication techniques (e.g., non-repeatability) and direct AM techniques (e.g., material selection), their use of viscous ceramic slurries constrains the geometries that are able to be realized. To mitigate scaffold feature-size limitations, we look to biomimetic mineralization as a means of coating polymeric scaffold patterns with a bioceramic.

Applying strategies found in biomineralization – the process by which living organisms secrete inorganic minerals to harden or stiffen existing tissues in the forms of skeletons, shells, teeth, etc. – biomimetic mineralization is the formation of new crystalline phase via nucleation followed by crystal growth in aqueous solutions at ambient conditions [57]. Biomimetic approaches to mineralization typically involve soaking the target in simulated body fluid (SBF) – an aqueous solution of salts that contains ions approximating those of human plasma [58]. SBF is supersaturated with respect to apatite, with the concentration of HCO_3^- influencing the mineral precipitates [59]. SBF has been used to deposit formations of bonelike apatite, which is essential for material to bond to living bone [60]. In addition, SBF coatings have good resorption [61] and have been shown to affect osteoblast viability, proliferation, and gene expression [62]. Coated implants and scaffolds have increased bone ingrowth (compared to non-treated implant) [63], biocompatibility [64], osteoconductive properties [58] and bone bonding [65]. In addition to creating a bone like apatite, and creating favorable conditions for bone growth, SBF has been used to mineralize several different materials: PLLA and PLGA [66], collagen [67], Ti6Al4V [68], Bioglass® [69].

The process chain is as follows (Figure 3):

1. *Fabrication of scaffold pattern:* A scaffold pattern with designed pore geometries is fabricated using additive manufacturing.
2. *Surface treatment of scaffold patterns:* Scaffold patterns are chemically treated to activate their surfaces to increase nucleation sites and to enhance the rate and quality of the mineral deposition.
3. *Mineralization of scaffold patterns:* The scaffold pattern is submerged in a simulated body fluid solution that deposits layers of biocompatible minerals (hydroxyapatite, HA) on its surface.
4. *Burnout and sintering of scaffold patterns:* The mineralized scaffold pattern is pyrolyzed to remove the pattern material and to sinter the deposited minerals, thus leaving behind a three-dimensional bioceramic scaffold.

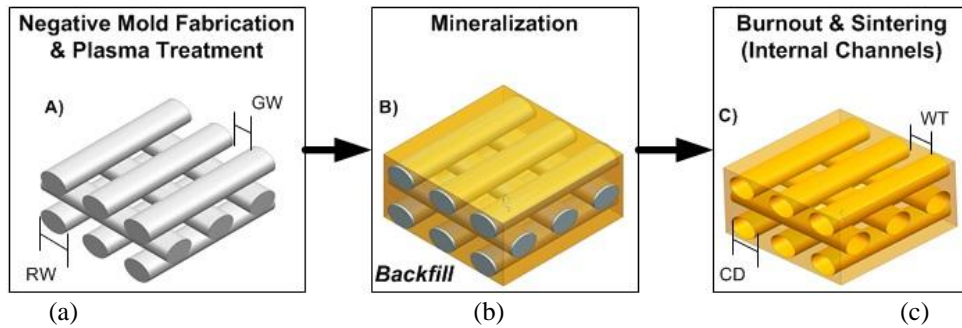


Figure 3. Indirect Scaffold Fabrication Process; a) scaffold pattern is fabricated by AM, b) scaffold pattern coated with bioceramic following mineralization, c) biocompatible scaffold formed after pyrolyzing pattern material

Like existing indirect AM scaffold fabrication techniques, this approach will alleviate geometric limitations typical of stochastic methods and the material limitations of direct AM methods. The biomimetic mineralization coating approach, however, uses a low-viscosity aqueous SBF solution, which the authors hypothesize will better penetrate complex scaffold geometries and thus eliminate the geometry and feature-size limitations found in existing indirect techniques.

4. EXPERIMENTAL METHODS

4.1 Pattern Fabrication via Fused Deposition Modeling

Extrusion-based processes, such as Fused Deposition Modeling (FDM), are popular choices for AM scaffold fabrication as the biopolymers that they selectively extrude are sufficiently stiff to span small gaps between scaffold struts, and thus eliminate the need for a secondary support material [25]. Scaffold porosity topology is altered by varying the thickness of the deposited lines (road width, RW), the offset distance between lines (gap width, GW), and the offset angle between each layer (Figure 3a).

In this work, the authors investigate two materials for the creation of scaffold materials: ABS (Stratasys P-400) and investment casting wax (ICW) material (Stratasys ICW-05). These are not necessarily ideal pattern materials; an ideal material would be receptive for the mineralization process and would be suitable for removal via pyrolysis (i.e., is able to be removed via a heat treatment without significant warping and toxic ash residue). However, they are sufficient for providing a proof of concept for the process. In addition, these two materials were shown to span small gaps and have been used successfully in other burnout processes [70-72].

Scaffold patterns are fabricated using a Stratasys FDM 1500 (ABS) and a Stratasys FDM 1600 (ICW) and a T12 nozzle (0.305 mm diameter). The scaffold fabrication printing parameters (i.e., road width (RW), road orientation, temperatures, etc.) used in experimentation are summarized in Table 1. Printed scaffold patterns were 12 mm in diameter, 1.5 mm in height and printed with a layer thickness of 0.30 mm (5 total layers).

Table 1. Pattern fabrication processing parameters

Material	Processing Temperature (Model/Support/Envelope)	Road Width (mm)	Road Orientation	Printing Pattern
ABS	270 / 265 / 270 °C	0.3	0-90°	Single roads
ICW	70 / 71 / 28 °C	0.4	0-90°	Continuous

4.2 Scaffold Surface Treatment

Mineralization via SBF does not typically result in cohesive coatings without a preliminary surface treatment of the polymeric substrate [26]. As such, the pattern must first undergo a surface treatment prior to mineralization. The authors investigated two candidate surface treatments:

- *Plasma treatment* activates surface groups for mineralization and decreases the contact angle allowing for aqueous solutions to easily penetrate the scaffold [73]. Plasma treatment has been successfully used in stochastic scaffold processes including PCL [74], and PCL-HA [73]. Samples are plasma treated in an oxygen environment for 15 minutes at 50 milliamperes in an SPI Plasma Prep II.

- *Sodium hydroxide (NaOH) etching* creates negatively charged groups on surfaces, and has shown to increase mineralization of treated surfaces when compared to identical, non-treated surfaces [58]. In this procedure, samples are immersed in 0.1M NaOH solution for 15 minutes.

4.3 Scaffold Mineralization

As described in Section 3, simulated body fluid (SBF) is used to biomimetically mineralize the scaffold patterns. A 10x concentrated SBF formulation (Table 2) is used in this process since higher concentrations accelerate the formation of minerals and are stable for long periods of time [59, 75]. 1x and 5x concentrations were explored in preliminary experiments, but did not result in sufficient mineral coating on the patterns' surfaces [26].

To prevent premature precipitation, two aqueous solutions are prepared: a “stock” solution containing all of the ions except for the bicarbonate, and another aqueous solution containing only the bicarbonate (Table 3). Precipitation occurs when the two solutions are mixed (10x SBF is prepared from the stock and bicarbonate solution in a 4:1 ratio). Scaffold patterns are then anchored to the center of a petri-dish containing mixed SBF. Fresh SBF is provided every two hours to ensure that ion concentration remains at a level that produces mineralization.

Table 2. Ion Concentrations (mM) of blood plasma and 10xSBF

Ion	Blood Plasma	10xSBF [74]
Na ⁺	142	1030.0
K ⁺	5.0	5.0
Cl ⁻	103	1065
Ca ²⁺	2.5	25
Mg ²⁺	1.05	5
H ₂ PO ₄ ⁻	1.0	10.0
SO ₄ ²⁻	0.5	--
HCO ₃ ⁻	27.0	10.0
pH	7.2-7.4	6.1

Table 3. Salt masses for stock and bicarbonate solutions.

	Salts	Grams
Stock Solution	NaCl	1.23
	KCl	3.73
	CaCl ₂ · 2H ₂ O	3.68
	MgCl ₂ · 6H ₂ O	3.05
	NaH ₂ PO ₄	1.20
Bicarbonate Solution	Na ₂ SO ₄	0.71
	NaHCO ₃	0.84

Two flow conditions (dynamic and static) are investigated to identify which would result in increased mineral deposits. Dynamic flows are tested to help mineralize the porous scaffolds by forcing fluid through them. For dynamic flow tests, the samples are placed on an orbital shaker (~70 Hz) inside an incubation chamber set at 37 °C.

4.4 Pattern Pyrolysis and Sintering

Once the scaffolds are successfully mineralized, they are placed in a furnace to burn away the polymeric pattern material (ABS or ICW). The heating profile used for ABS patterns is based on thermogravimetric analysis (TGA) of ABS by ToolworX and Stratasys Inc. [76]. Through this analysis it was found that ~95% of ABS is removed at ~450 °C, while the remaining material removed at 575 °C [71]. Similarly, the heating profile for Stratasys ICW-06 was based on research on bioceramic implants that used ICW-06 as a binder in a FDC processes. Bose et al. heated bioceramic implants up to 550 °C to evaporate the mold and binder and chose a slow heating rate of 2°C/min to avoid cracking or distortion of the part [77]. A slow heating rate (0.5 °C /min) was used to prevent cracking and distortion of the part.

The sintering temperature chosen for both ABS and ICW samples in this study is 800 °C (with a 1 hour hold) at a rate of 0.5 °C/min.

5. RESULTS AND DISCUSSION

5.1 Determining Surface Treatment and Flow Conditions for Scaffold Mineralization

Critical to the development of this indirect scaffold fabrication process, is the identification of mineralization processing parameters that significantly increase mineral deposition. With SBF concentration determined, the surface treatment and flow type during mineralization were treated as variables to identify the combination which provided the best mineralization. A total of 8 scaffold samples, featuring permutations of ABS and ICW patterns, Plasma and NaOH surface treatments, and dynamic and static flows, were created and weighed before and after mineralization to determine the amount of materials deposited. The final mass of deposited minerals for each scaffold is presented in Table 4.

A three-way ANOVA was performed on the mineral mass data [78]. The analysis indicated that flow condition and surface treatment were the two most significant factors in this experiment (F-ratios of 170 and 10.2), while the scaffold material had only a small effect (F-ratio of 1.89). The calculated p-values, which indicate confidence in our hypothesis, were 0.0486 and 0.194 (for the flow condition and surface treatment parameters, respectively), and indicate a strong relation between the experimental factors and amount of mineral deposition.

As can be seen in Table 4, scaffolds that were plasma treated mineralized more than those treated with NaOH. Also, dynamic conditions resulted in much better mineralization than static conditions (a 77.2-96.3% increase). As such, all further experiments were conducted using the plasma surface treatment and dynamic flow conditions.

Table 4. Mineral mass data (in grams)

	ABS	ICW	
Dynamic	0.0153	0.0141	Plasma
	0.0108	0.0109	NaOH
Static	0.0033	0.0026	Plasma
	0.0030	0.0004	NaOH

5.2 Process Results

To validate the presented approach, patterns were fabricated from ABS and ICW with gap widths (GW) of 500 μm . Following mineralization and sintering, these GW measurements will correspond to the wall thickness (WT) of the scaffold (Figure 3). Similarly, the internal channel diameter (CD) will be formed when the RW material is removed during sintering and will have a diameter of $\sim 300 \mu\text{m}$ and $\sim 400 \mu\text{m}$ for ABS and ICW patterns respectively (Table 1). Sample printed patterns are presented in Figure 4. As can be seen, the diameter of the RW for ICW is not constant. The low viscosity of the extruded wax causes the roads to sag when spanning gaps; roads swell (when supported) and thin (when unsupported), creating a wave-like pattern along the length of their deposition.

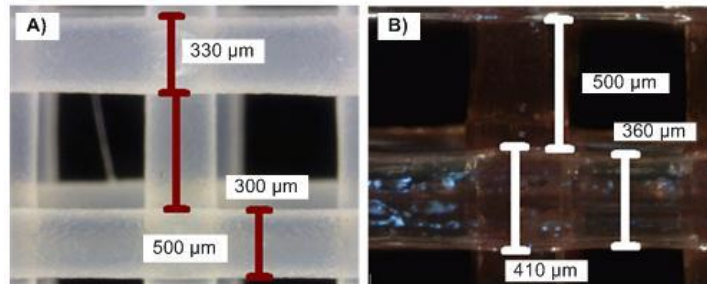


Figure 4. A) ABS and B) ICW scaffold patterns with a 500 μm gap width

ABS and ICW scaffolds were plasma treated (Section 4.2) and then mineralized in a 10xSBF solution for 48 hours under dynamic flow conditions. Fracture surfaces of mineralized ABS and ICW samples are presented in Figure 5.

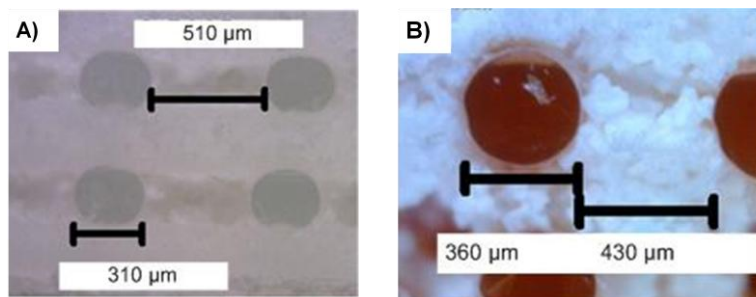


Figure 5. Fracture surface of pre-sintered scaffolds with GW = 500 μm ; (a) ABS, (b) ICW

Following mineralization, scaffolds were dried overnight and then sintered to 800 $^{\circ}\text{C}$ at a rate of 0.5 $^{\circ}\text{C}/\text{min}$. The mass of the samples were recorded before and after mineralization, and after sintering, to determine the amount of mineral deposition and to verify that the polymer pattern had been removed. Fracture surfaces of sintered samples with a GW = 500 μm are presented in Figure 6. As can be seen, the patterns' original pores (now the scaffold walls) are filled with mineral as desired.

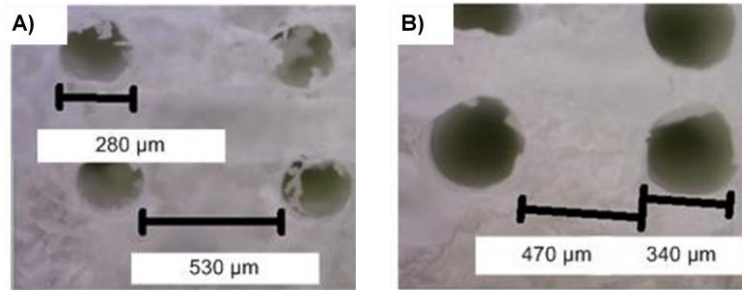


Figure 6. Fracture surface of sintered scaffolds with GW = 500 μm; (a) ABS, (b) ICW

Measurements of wall thickness (WT) and channel diameter (CD) were made following printing and following mineralization and sintering. Measurements of the samples with 500 μm are presented in Table 5. The “Pre-Sintered” values fall within the range of expected values (i.e., the “Pre-Mineralized” values), except for the ICW WT. Plasma treatment may have caused this area of the scaffold to deform, resulting in a smaller reported WT. A slight shrinkage during the burnout and sintering process is noted, which causes the CD to decrease slightly.

Table 5. Wall thickness and channel diameter measurements for samples with GW = 500 μm

	Designed		Printed		Mineralized and Sintered	
	GW / WT (μm)	RW / CD (μm)	GW / WT (μm)	RW / CD (μm)	WT (μm)	CD (μm)
ABS	500	300	510	310	530	280
ICW	500	400	430	360	470	340

To explore the hypothesis that mineralization via an aqueous SBF solution would be able to create finer scaffold features than existing indirect processes, additional ICW samples with gap widths of 150 μm and 300 μm were fabricated. As can be seen in the images from field-emission scanning electron microscopy (FE-SEM) of the fracture surface of the scaffold, the SBF mineralization approach is able to deposit minerals in gaps as small as 150 μm (Figure 7). The resulting wall thickness from these scaffolds was 158 ± 33.4 μm.

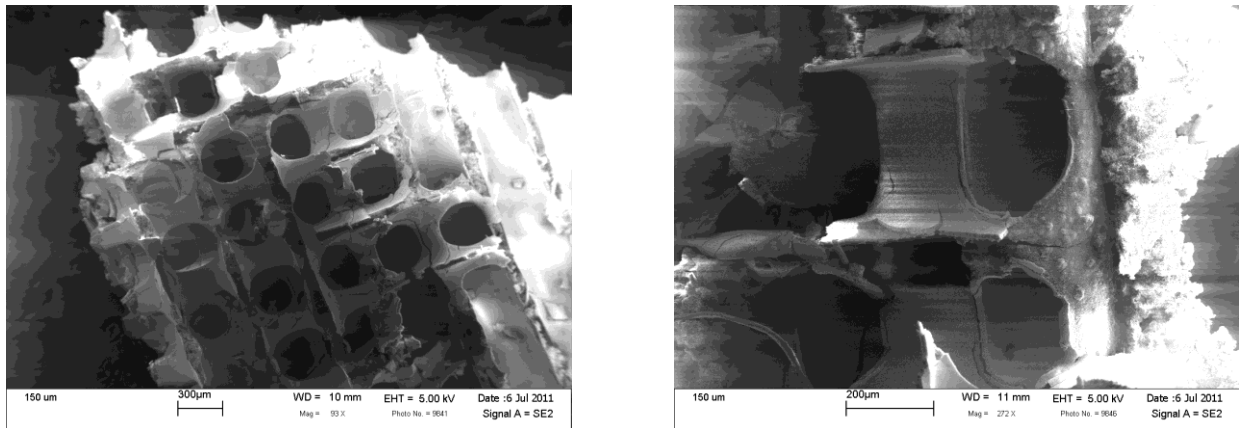


Figure 7. FE-SEM images of mineralized scaffold with wall thickness = 150 μm

To benchmark the presented method against existing indirect fabrication methods, Detsch and coauthors’ scaffold fabrication process (highlighted row of Table 6) was selected as a benchmark since it has produced the smallest WT and CT features thus far in the literature. All fabrication methods were compared to the benchmark CD and WT values and assigned either a “0,” “+,” or “-” based on if they had an equal, better or worse feature resolution (Table 6). The WT and CD values obtained from the fabrication process presented here (first two rows of Table 6) met or exceeded the resolution of other indirect methods.

Table 6. Comparison of WT and CD across existing indirect scaffold fabrication processes

<i>Mold Fabrication</i>	<i>Mold Material</i>	<i>Cast Material</i>	<i>Measured[†]</i>		<i>Compared</i>		<i>Reference</i>
			<i>WT</i>	<i>CD</i>	<i>WT</i>	<i>CD</i>	
FDM: FDM1500	ABS	10xSBF	530	280	–	+	Figure 6
FDM: FDM1600	ICW	10xSBF	158	340	+	–	Figure 7
D-IJP: Solidscape MM2	Wax	PGA, PLA, HA	~500	500- 800	0	–	[55]
SLA: 3D Systems	Cibatool SL5170	HA slurry	560- 755	366- 968	–	–	[49]
D-IJP: Solidscape BT66	Wax	HA slurry	~500	~300	0	0	[51]

[†] All measurements are in micrometers

To chemically characterize the fabricated scaffolds, energy-dispersive X-ray spectroscopy (EDS) was completed on 12 different spots on the 150 μm samples. EDS detected elements in all samples of calcium and phosphorous, with an average Ca/P ratio = 1.7 ± 0.52 . While it is difficult to speculate on the nature of mineral based on Ca/P ratio alone, it can be concluded with certainty that the mineral consists of calcium and phosphorous only, as other elements like magnesium and sodium were not detected. A Ca/P ratio of 1.7 indicates that it is slightly higher than that for hydroxyapatite (1.67), but is quite comparable. Therefore, we can speculate that the mineral formed is a type of hydroxyapatite, is probably crystalline in nature, and is not very soluble in aqueous environments. This also suggests that the surfaces may be osteoconductive and may promote growth and proliferation of bone-like cells. However, X-ray diffraction is needed to confirm the results of EDS.

6. CLOSURE AND FUTURE WORK

In this work, the authors present an indirect scaffold fabrication process similar to investment casting wherein polymer scaffold patterns are coated in a bioceramic via a biomimetic mineralization process. The patterns are first fabricated by Fused Deposition Modeling (from either ABS or investment casting wax materials). The surfaces of the patterns are then chemically treated to activate their surfaces to increase nucleation sites and to enhance the rate and quality of the mineral deposition. The scaffold pattern is then submerged in a simulated body fluid solution that deposits layers of biocompatible minerals on its surface. Finally, the mineralized scaffold pattern is pyrolyzed to remove the pattern material and to sinter the deposited minerals, thus leaving behind a three-dimensional bioceramic scaffold.

Critical to the development of this indirect scaffold fabrication process was the identification of mineralization processing parameters that would significantly increase mineral deposition. Using ANOVA, surface treatment and flow conditions were identified as significant mineralization factors compared to pattern material type. Plasma surface treatment and dynamic flow conditions were found to be ideal processing conditions and resulted in increased mineralization.

The internal architecture of the fabricated scaffolds was characterized by the wall thickness (WT) and channel diameter (CD) and was benchmarked against existing indirect scaffold fabrication processes. Although the smallest CD achieved was limited by the road width of the FDM process (~280 μm), it is slightly better than the 300 μm pores created by a direct inkjet printing process. The wall thicknesses achieved by the process were as small as 158 μm – ~30% smaller than that achieved by existing indirect approaches. This fine feature size suggests that the biomimetic mineralization coating approach, which uses a low-viscosity aqueous SBF solution, alleviates the geometry and feature-size limitations found in existing indirect techniques that rely on viscous ceramic slurries.

In future work, the authors look to perform cell viability and mechanical testing of the scaffolds. Qualitatively, the mineral structure seems too weak for applications other than maxillofacial implantation. In addition, the authors will investigate creating patterns with a biocompatible polymer, such as PCL, to mitigate concerns of ash residue from the polymers studied here. Furthermore, the authors will investigate the use of a direct inkjet printing AM process, such as the Objet PolyJet process, as a means for fabricating scaffolds with designed mesostructure. Such a process would alleviate the geometric limitations found in extrusion processes, which are limited to simple overlapping of parallel roads (aka “log piles”) [79] with a fixed height between layers [80].

Finally, the authors would like to further explore the crystalline surface structure that results from the mineralization approach. It is believed that there exist nano-sized topographical features that might influence cell adhesion and orientation. In addition, the resulting scaffold surface will likely provide micro-pores in addition to the designed macro-pores. This gradient porosity, which will be created without particle leaching, has been shown to be beneficial as larger pores increase nutrient diffusion while the smaller pores provide living spaces for cells [55].

7. ACKNOWLEDGEMENTS

The authors acknowledge Dr. Aaron Goldstein, of the Virginia Tech Department of Chemical Engineering, for his suggestions and insight in the biomimetic mineralization process. We also acknowledge the Institute for Critical Technologies and Applied Science (ICTAS) Nanoscale Characterization and Fabrication Laboratory (NCFL) at Virginia Tech for support with FE-SEM imaging.

8. REFERENCES

1. Hutmacher, D.W., *Scaffolds in tissue engineering bone and cartilage*. Biomaterials, 2000. **21**(24): p. 2529-2543.
2. Mikos, A.G., et al., *Prevascularization of porous biodegradable polymers*. Biotechnology and Bioengineering, 1993. **42**(6): p. 716-723.
3. JEFFREY O. HOLLINGER and JOHN P. SCHMITZ, *Macrophysiologic Roles of a Delivery System for Vulnerary Factors Needed for Bone Regeneration*. Annals of the New York Academy of Sciences, 1997. **831**(Bioartificial Organs: Science, Medicine, and Technology): p. 427-437.
4. António J. Salgado, O.P.C., Rui L. Reis., *Bone Tissue Engineering: State of the Art and Future Trends*. Macromolecular Bioscience, 2004. **4**(8): p. 743-765.
5. Drury, J.L. and D.J. Mooney, *Hydrogels for tissue engineering: scaffold design variables and applications*. Biomaterials, 2003. **24**(24): p. 4337-4351.
6. Andreas Pfister, R.L., Andres Laib, Ute Hübner, Rainer Schmelzeisen, Rolf Mülhaupt., *Biofunctional rapid prototyping for tissue-engineering applications: 3D bioplotting versus 3D printing*. Journal of Polymer Science Part A: Polymer Chemistry, 2004. **42**(3): p. 624-638.
7. Hutmacher, D.W., *Scaffold design and fabrication technologies for engineering tissues - state of the art and future perspectives*. Journal of Biomaterials Science -- Polymer Edition, 2001. **12**: p. 107-124.
8. Kneser, U., Scafer, D.J., Munder, B., Klemt, C., Andree, C., Stark, G. B., , *Tissue Engineering bone*. Minimally Invasive Therapy & Allied Technologies, 2002. **11**(3): p. 107-116.
9. Zeltinger, J., et al., *Effect of Pore Size and Void Fraction on Cellular Adhesion, Proliferation, and Matrix Deposition*. Tissue Engineering, 2001. **7**(5): p. 557-572.
10. van Tienen, T.G., et al., *Tissue ingrowth and degradation of two biodegradable porous polymers with different porosities and pore sizes*. Biomaterials, 2002. **23**(8): p. 1731-1738.
11. Karande, T.S., J.L. Ong, and C.M. Agrawal, *Diffusion in Musculoskeletal Tissue Engineering Scaffolds: Design Issues Related to Porosity, Permeability, Architecture, and Nutrient Mixing*. Annals of Biomedical Engineering, 2004. **32**(12): p. 1728-1743.
12. Burg, K.J.L., S. Porter, and J.F. Kellam, *Biomaterial developments for bone tissue engineering*. Biomaterials, 2000. **21**(23): p. 2347-2359.
13. Hollinger, J., *Factors for Osseous Repair and Delivery: Part II*. Journal of Craniofacial Surgery, 1993. **4**(3): p. 135-141.
14. Li, S., et al., *Macroporous biphasic calcium phosphate scaffold with high permeability/porosity ratio*. Tissue Engineering, 2003. **9**(3): p. 535-548.
15. Leong, K.F., C.M. Cheah, and C.K. Chua, *Solid freeform fabrication of three-dimensional scaffolds for engineering replacement tissues and organs*. Biomaterials, 2003. **24**(13): p. 2363-2378.
16. Ann Park and Linda Griffith Cima, *In vitro cell response to differences in poly-L-lactide crystallinity*. Journal of Biomedical Materials Research, 1996. **31**(1): p. 117-130.
17. Ng, K.W., H.L. Khor, and D.W. Hutmacher, *In vitro characterization of natural and synthetic dermal matrices cultured with human dermal fibroblasts*. Biomaterials, 2004. **25**(14): p. 2807-2818.
18. Brekke, J.H., *A Rationale for Delivery of Osteoinductive Proteins*. Tissue Engineering, 1996. **2**(2): p. 97-114.

19. Mikos, A., et al., *Preparation and characterization of poly (L-lactic acid) foams*. Polymer, 1994. **35**(5): p. 1068-1077.
20. Mooney, D., et al., *Novel approach to fabricate porous sponges of poly (-lactic-co-glycolic acid) without the use of organic solvents*. Biomaterials, 1996. **17**(14): p. 1417-1422.
21. Harris, L., B. Kim, and D. Mooney, *Open pore biodegradable matrices formed with gas foaming*. Journal of Biomedical Materials Research Part A, 1998. **42**(3): p. 396-402.
22. Wei, G. and P.X. Ma, *Structure and properties of nano-hydroxyapatite/polymer composite scaffolds for bone tissue engineering*. Biomaterials, 2004. **25**(19): p. 4749-4757.
23. Oliveira, J.M., et al., *Novel hydroxyapatite/chitosan bilayered scaffold for osteochondral tissue-engineering applications: Scaffold design and its performance when seeded with goat bone marrow stromal cells*. Biomaterials, 2006. **27**(36): p. 6123-6137.
24. Lloyd, D.R., K.E. Kinzer, and H.S. Tseng, *Microporous membrane formation via thermally induced phase separation. I. Solid-liquid phase separation*. Journal of Membrane Science, 1990. **52**(3): p. 239-261.
25. Yong, W.Y., et al., *Rapid prototyping in tissue engineering: challenges and potential*. TRENDS in Biotechnology, 2004. **22**(12): p. 643-652.
26. Bernardo, J., et al., *Towards Indirect Scaffold Fabrication via Additive Manufacturing and Hydroxyapatite Mineralization*, in *International Solid Freeform Fabrication Symposium*. 2010: Austin, TX.
27. Lam, C.X.F., *Scaffold development using 3D printing with a starch-based polymer*. Materials Science Engineering, 2002. **20**: p. 49-56.
28. Kim, S.S., et al., *Survival and function of hepatocytes on a novel three-dimensional synthetic biodegradable polymer scaffold with an intrinsic network of channels*. Annals of Surgery, 1998. **228**(1): p. 8-13.
29. Levy, R.A., *CT-generated porous hydroxyapatite orbital floor prosthesis as a prototype bioimplant*. American Journal of Neuroradiology, 1997. **18**: p. 1522-1525.
30. Porter, N.L., *Fabrication of porous calcium polyphosphate implants by solid freeform fabrication: A study of processing and in vitro degradation characteristics*. Journal of Biomedical Materials Research, 2001. **56**: p. 504-515.
31. Cooke, M.N., et al., *Use of stereolithography to manufacture critical-sized 3D biodegradable scaffolds for bone ingrowth*. Journal of Biomedical Materials Research, 2003. **64B**(2): p. 65-69.
32. Liu, V.A. and S.N. Bhatia, *Three-Dimensional Photopatterning of Hydrogels Containing Living Cells*. Biomedical Microdevices, 2002. **4**(4): p. 257-266.
33. Lee, G., et al. *Biocompatibility of SLS-formed Calcium Phosphate Implants*. in *Proceedings of the International Solid Freeform Fabrication Symposium*. 1996. Austin, TX.
34. Lee, G. and J. Barlow. *Selective laser sintering of bioceramic materials for implants*. in *Proceedings of the International Solid Freeform Fabrication Symposium*. 1993. Austin, TX.
35. Tan, K.H., et al., *Scaffold development using selective laser sintering of polyetheretherketone-hydroxyapatite biocomposite blends*. Biomaterials, 2003. **24**(18): p. 3115-3123.
36. Chu, T.M.G., et al., *Mechanical and in-vivo performance of hydroxyapatite implants with controlled architectures*. Biomaterials, 2002. **23**: p. 1283-1293.
37. Yeong, W.Y., et al., *Rapid prototyping in tissue engineering: challenges and potential*. TRENDS in Biotechnology, 2004. **22**(12): p. 643-652.
38. Chua, C.K., et al., *Development of tissue scaffolds using selective laser sintering of polyvinyl alcohol/hydroxyapatite biocomposite for craniofacial and joint defects*. Journal of Material Science: Materials in Medicine, 2004. **15**: p. 1113 - 1121.
39. Tan, K.H., et al., *Scaffold development using selective laser sintering of polyetheretherketone-hydroxyapatite biocomposite blends*. Biomaterials, 2003. **24**(18): p. 3115 - 3123.
40. Porter, N.L., R.M. Pilliar, and M.D. Grynblas, *Fabrication of porous calcium polyphosphate implants by solid freeform fabrication: A study of processing parameters and in vitro degradation characteristics*. Journal of Biomedical Materials Research, 2001. **56**(4): p. 504-515.
41. Levy, R., et al., *CT-generated porous hydroxyapatite orbital floor prosthesis as a prototype bioimplant*. American Journal of Neuroradiology, 1997. **18**(8): p. 1522.
42. Griffith, M.L. and J.W. Halloran, *Freeform Fabrication of Ceramics via Stereolithography*. Journal of the American Ceramic Society, 1996. **Vol. 79**(No. 10): p. pp. 2601-2608.
43. Cesarano III, J., *Robocasting of Ceramics and Composites Using Fine Particle Suspensions*. 1999. Medium: P; Size: 10 pages.

44. Cesarano III, J., R. Segalman, and P. Calvert, *Robocasting provides moldless fabrication from slurry deposition*. Ceramic Industry, 1998. **148**(4): p. 94.
45. Griffith, M.L. and J.W. Halloran, *Scattering of Ultraviolet Radiation in Turbid Suspensions*. Journal of Applied Physics, 1997. **Vol. 81**(No. 6): p. pp. 2538-2546.
46. Cesarano III, J. *A review of robocasting technology*. 1999.
47. Miranda, P., et al., *Sintering and robocasting of [beta]-tricalcium phosphate scaffolds for orthopaedic applications*. Acta Biomaterialia, 2006. **2**(4): p. 457-466.
48. Lee, M., J. Dunn, and B. Wu, *Scaffold fabrication by indirect three-dimensional printing*. Biomaterials, 2005. **26**(20): p. 4281-4289.
49. Chu, T., et al., *Hydroxyapatite implants with designed internal architecture*. Journal of Materials Science: Materials in Medicine, 2001. **12**(6): p. 471-478.
50. Yeong, W., et al., *Indirect fabrication of collagen scaffold based on inkjet printing technique*. Rapid Prototyping Journal, 2006. **12**(4): p. 229-237.
51. Detsch, R., et al., *3D-Cultivation of bone marrow stromal cells on hydroxyapatite scaffolds fabricated by dispense-plotting and negative mould technique*. Journal of Materials Science: Materials in Medicine, 2008. **19**(4): p. 1491-1496.
52. Sachlos, E., et al., *Novel collagen scaffolds with predefined internal morphology made by solid freeform fabrication*. Biomaterials, 2003. **24**(8): p. 1487-1497.
53. Chrisey, D.B., *The Power of Direct Writing*. Science, 2000. **289**(5481): p. 879.
54. Dellinger, J.G., C. Joseph, III, and D.J. Russell (2007) *Robotic deposition of model hydroxyapatite scaffolds with multiple architectures and multiscale porosity for bone tissue engineering*. Journal of Biomedical Materials Research Part A, 383-394 DOI: 10.1002/jbm.a.31072.
55. Taboas, J., et al., *Indirect solid free form fabrication of local and global porous, biomimetic and composite 3D polymer-ceramic scaffolds*. Biomaterials, 2003. **24**(1): p. 181-194.
56. Hutmacher, D.W., M. Sittinger, and M.V. Risbud, *Scaffold-based tissue engineering: rationale for computer-aided design and solid free-form fabrication systems*. Trends in Biotechnology, 2004. **22**(7): p. 354-362.
57. Xu, A.-W., Y. Ma, and H. Colfen, *Biomimetic Mineralization*. Journal of Materials Chemistry, 2006. **17**: p. 415-4549.
58. Kretlow, J. and A. Mikos, *Review: mineralization of synthetic polymer scaffolds for bone tissue engineering*. Tissue Engineering, 2007. **13**(5): p. 927-938.
59. Müller, L. and F.A. Müller, *Preparation of SBF with different content and its influence on the composition of biomimetic apatites*. Acta Biomaterialia, 2006. **2**(2): p. 181-189.
60. Kokubo, T. and H. Takadama, *How useful is SBF in predicting in vivo bone bioactivity?* Biomaterials, 2006. **27**(15): p. 2907-2915.
61. Leeuwenburgh, S., et al., *Osteoclastic resorption of biomimetic calcium phosphate coatings in vitro*. Journal of Biomedical Materials Research, 2001. **56**(2): p. 208-215.
62. Chou, Y.-F., et al., *The effect of biomimetic apatite structure on osteoblast viability, proliferation, and gene expression*. Biomaterials, 2005. **26**(3): p. 285-295.
63. Barrère, F., et al., *Osteointegration of biomimetic apatite coating applied onto dense and porous metal implants in femurs of goats*. Journal of Biomedical Materials Research Part B: Applied Biomaterials, 2003. **67B**(1): p. 655-665.
64. Jalota, S., S.B. Bhaduri, and A.C. Tas, *Osteoblast proliferation on neat and apatite-like calcium phosphate-coated titanium foam scaffolds*. Materials Science and Engineering: C, 2007. **27**(3): p. 432-440.
65. Yan, W.Q., et al., *Bonding of chemically treated titanium implants to bone*. Journal of Biomedical Materials Research, 1997. **37**(2): p. 267-275.
66. Zhang, R. and P. Ma, *Biomimetic polymer/apatite composite scaffolds for mineralized tissue engineering*. Macromolecular Bioscience, 2004. **4**(2): p. 100-111.
67. Lickorish, D., et al., *Collagen-hydroxyapatite composite prepared by biomimetic process*. Journal of Biomedical Materials Research Part A, 2004. **68A**(1): p. 19-27.
68. Tas, A. and S. Bhaduri, *Rapid coating of Ti6Al4V at room temperature with a calcium phosphate solution similar to 10× simulated body fluid*. J Mater Res, 2004. **19**(9): p. 2742-2749.
69. Kokubo, T., *Surface chemistry of bioactive glass-ceramics*. Journal of Non-Crystalline Solids, 1990. **120**(1-3): p. 138-151.
70. Lee, C., et al., *Rapid investment casting: direct and indirect approaches via fused deposition modelling*. The International Journal of Advanced Manufacturing Technology, 2004. **23**(1): p. 93-101.

71. ToolworX, R. and S. Inc, *Investment Casting Using FDM/ABS Rapid Prototype Patterns*.
72. Bandyopadhyay, A., S. Danforth, and A. Safari, *Effects of processing history on thermal debinding*. Journal of Materials Science, 2000. **35**(16): p. 3983-3988.
73. Venugopal, J., et al., *Electrospun-modified nanofibrous scaffolds for the mineralization of osteoblast cells*. Journal of Biomedical Materials Research Part A, 2008. **85**(2): p. 408-417.
74. Yang, F., J. Wolke, and J. Jansen, *Biomimetic calcium phosphate coating on electrospun poly (-caprolactone) scaffolds for bone tissue engineering*. Chemical Engineering Journal, 2008. **137**(1): p. 154-161.
75. Li, J., et al., *Transfer of apatite coating from porogens to scaffolds: Uniform apatite coating within porous poly(DL-lactic-co-glycolic acid) scaffold in vitro*. Journal of Biomedical Materials Research Part A, 2007. **80A**(1): p. 226-233.
76. Yang, M.-H., *The thermal degradation of acrylonitrile-butadiene-styrene terpolymer under various gas conditions*. Polymer Testing, 2000. **19**(1): p. 105-110.
77. Bose, S., M. Avila, and A. Bandyopadhyay. *Processing of bioceramic implants via fused deposition process*. 1998.
78. Bernardo, J., *Indirect Tissue Scaffold Fabrication via Additive Manufacturing and Biomimetic Mineralization*, in *Mechanical Engineering*. 2010, Virginia Tech: Blacksburg, VA.
79. Grida, I. and J.R.G. Evans, *Extrusion Freeforming of Ceramics through Fine Nozzles*. Journal of European Ceramic Society, 2003. **Vol. 23**: p. pp. 629-635.
80. Tsang, V.L. and S.N. Bhatia, *Fabrication of Three-Dimensional Tissues*. Advances in Biochemical Engineering Biotechnology, 2006. **103**: p. 189-205.